ARTICLE NO. 80-4083

G80-073

Low-Cost Autonomous Navigation Method for Moderate-g Missions

00016
00022

Shmuel J. Merhav*
Technion—Israel Institute of Technology, Haifa, Israel

This paper describes a low-cost inertial navigation system concept for a broad class of flight missions characterized by moderate accelerations and limited attitude variations. A novel hybrid mechanization, partially gimballed and partially strapdown, is presented. Implemented by an unbalanced two-axis gimbal system controlled by a two-degree-of-freedom gyro, the gimbal torquers provide locally level two-axis acceleration information. Pitch and roll measurements are provided by the gimbal pickoffs and heading information by a second gyro mounted in the inner gimbal. The dispensing of accelerometers and the simplified mechanization and computation imply a substantial saving in cost and potential improvement of reliability.

Nomenclature

A_x, A_y	= gain factors
d	= gyro drift rate
F	= specific force vector
F_E, F_N, F_V	= east, north, and vertical components of specific force
g	= net gravity vector
G	= index of geographical coordinate frame
H	= angular momentum
I	= moment of inertia, identity matrix
J	= moment of inertia
M_x, M_y	= torques on x and y axes
n	= spin speed of gyro rotor
R	= distance of vehicle from center of the Earth
s	= Laplace operator
T	= 3×3 orthogonal transformation matrix
u	= normalized position or velocity divergence
$V_G, \dot{V}_G$	= velocity and acceleration in geographical coordinates
V_E, V_N, V_V	= east, north, and vertical components of velocity
λ	= latitude
ϕ, θ, ψ	= airframe roll pitch and yaw angles
$[\phi]_x, [\psi]_z, [\theta]_y$	= 3×3 Euler transformations with respect to x,y,z axis
$[\psi]$	= 2×2 coordinate transformation with respect to ψ
ω	= angular rate vector
ω_s	= Schuler frequency
Ω_s	= sidereal rate of rotation of the Earth
σ	= standard deviation
η, ξ	= gimbal pitch and roll angles
ψ_A, ψ_E, ψ_N	= small platform angular errors with respect to the vertical, east, and north axes

I. Introduction

AUTONOMOUS navigation, which by definition excludes all kinds of external aids, is essentially based on inertial instrumentation, except for the crudest heading and velocity methods using magnetic and airspeed measurements. Originally developed for ballistic missiles and military aircraft with all attitude and high-g capability, the technology in a state-of-the-art inertial navigation system (INS) of the 1 n.mi./h class incurs high cost which often precludes its use in a wide scope of applications such as general aviation, helicopters, RPV's, and ground vehicles. The principal common factor is their low-g environment and limited attitude requirement. These conditions can be advantageously used in the choice of sensors and inertial measurement unit (IMU) mechanization so as to achieve a substantial reduction in cost and complexity.

Efforts to reduce cost and size and improve reliability have, in the past decade, been largely oriented to strapdown mechanizations.[1] However, the advantages expected from dispensing with the gimbal system are largely offset by the greater demands on gyroscopes and increased computational volume and speed. The greater sensitivity of strapdown systems to alignment errors[2] and to correlated noise components in the accelerometers and gyroscopes[3] have so far impeded their successful competition with gimballed systems in the 1 n.mi./h class.[1,2] Alternative approaches for improvement in cost effectiveness appear to involve a major departure from classical inertial navigation principles, or a new concept in its instrumentation. Examples of such departures have recently been reported. By constructing an optimal observer[4] on the (known) parameters of the aircraft, velocities are estimated from attitude and altitude measurements. The method appears to be potentially suitable for short-term autonomous navigation, but further work is needed with regard to sensitivity to parameter variations, trim errors, and wind modelling. An attempt to dispense with gyroscopes has recently been reported by Monaco et al.[5] A single-axis physical pendulum is Schuler tuned by measuring its angular acceleration, and the required immense moment of inertia is artificially provided by a torque motor driven by the highly amplified angular acceleration signal. The excessive gain ($\sim 10^7$) and gain stability required in its realization raise doubts as to its performance in an actual flight environment. An earlier attempt to depart from conventional IMU instrumentation by dispensing with the accelerometers has been reported by Hector[6] and Astrom and Hector.[7] Instead of a simple pendulum, a gryo-pendulum is Schuler tuned, again requiring excessive gains for the torquing commands. A detailed design and error analysis of this concept has been reported by Koenke,[8] verifying that the system obeys the basic laws of error propagation in INS's.

The foregoing examples reflect the continuing search for low cost navigation in the 1 n.m./h class for which the

Received Aug. 17, 1979; revision received Jan. 14, 1980.

Index categories: Navigation, Communication, and Traffic Control; Guidance and Control.

*Professor, Dept. of Aeronautical Engineering. Member AIAA.

technologies of conventional IMU's, originally developed for military applications, may be highly overdesigned. In the IMU configuration presented in this paper, a substantial reduction in the number of inertial sensors is achieved without departing from the basic principles of inertial navigation, e.g., as in Ref. 4, or resorting to new instrumentation concepts as in Ref. 5. It is shown that the gimballed and strapdown concepts can be combined into a hybrid mechanization using two gimbals and dispensing with the accelerometers. This hybrid mechanization apparently has significant advantages in cost effectiveness over both the gimballed and strapdown mechanizations. These advantages are, however, subject to the following assumptions: moderate accelerations which circumvent excessive gimbal torquer requirements; limited pitch variations which permit a simple gimbal mechanization; moderate steady-state yaw variations which prevent excessive temperature fluctuations in the gyro torquers; and moderate altitudes and velocities which simplify the navigation computations and reduce iteration rates. The method is investigated by modelling the dynamics, controls, and error sources in the sensors and the system, and by statistical analysis of the error propagation for flight durations of 1 h. The results demonstrate that a performance of the order of 1 n.m./h rms can be achieved.

II. System Considerations

In this section, INS mechanizations are reviewed in the light of the assumptions and requirements characterizing moderate-g missions and limited pitch requirement.

A. Assumptions and Requirements

1) The specific forces acting on the vehicle do not exceed the order of 1 g.

2) Attitudes are not limited except in pitch, which is limited to $\sim \pm 60$ deg.

3) Yaw rate, except for short durations, is assumed not to exceed values in the order of 10 deg/s.

4) Altitudes and velocities are moderate and typical of general aviation, helicopters, etc.

5) Navigation is implemented in conventional spherical coordinates.

6) The gravity vector is a known constant throughout the flight mission.

7) Duration of a typical autonomous flight phase does not exceed 1 h.

8) Altitude information is derived from conventional altimeters.

9) The navigation error should not exceed the order of 1 n.mi.

B. Review of Mechanization Problems

The basic mechanization problems will now be reviewed in the light of the preceding assumptions.

1. Navigation Equations

The standard navigation equations expressed in geographic coordinates are given in Ref. 3. In view of assumption 8, V_V can be derived from independent measurement of altitude h, so that the navigation equation reduces to

$$\begin{bmatrix} \dot{V}_N \\ \dot{V}_E \end{bmatrix} = \begin{bmatrix} F_N \\ F_E \end{bmatrix} + \begin{bmatrix} -\left(2\Omega_s \sin\lambda + \frac{V_E}{R}\tan\lambda\right) V_E + \frac{V_N V_V}{R} \\ \left(2\Omega_s \sin\lambda + \frac{V_E}{R}\tan\lambda\right) V_N + 2\Omega_s V_V \cos\lambda + \frac{V_E V_V}{R} \end{bmatrix} \tag{1}$$

in which V_V is now a time-varying parameter, and λ is determined from integration of $\dot{\lambda} = V_N/R$.

Measures of F_N and F_E, normally obtained from onboard accelerometers, are mounted in a coordinate frame (X_a, Y_a, Z_a). The measured specific force vector $F_a = [F_{xa}, F_{ya}, F_{za}]^T$ must be transformed to yield F_N and F_E. The three fundamental aspects of inertial navigation emerging from Eq. (1) are: 1) instrumentation—by which the specific force vector F is measured in an airborne coordinate frame defining F_a; 2) transformation—by which these measurements are transformed into the desired locally level geographical coordinate system, $F_G = T_{G/a} F_a$; 3) navigational computation—by which Eq. (1) is integrated to yield V_N, V_E and, by further integration, vehicle position X_G, Y_G.

2. Instrumentation

Specific Force Measurement: By assumption 1, the required measurement range is 1 g, and by assumption 9, the allowable null point uncertainty should not exceed 100 μg. Thus, the dynamic range is of the order of 10^4 instead of 10^5 or 10^6 in military or transatlantic missions. This reduction in dynamic range is a key feature in the realization of the low-cost IMU described later.

Platform Orientation Error: For unaccelerated motion along the vertical axis, $\dot{V}_V = 0$ in eq. (1), the specific force vector acting on the vehicle is $F = [F_N, F_E, -g]^T$. An orientation error vector $\Psi = [\psi_A, \psi_E, \psi_N]^T$ causes the error $\Delta F_G = [\Delta F_N, \Delta F_E, \Delta F_V]^T$. By Eq. (1), only ΔF_N and ΔF_E are relevant and can be expressed by

$$\begin{bmatrix} \Delta F_N \\ \Delta F_E \end{bmatrix} = \psi_A \begin{bmatrix} F_E \\ -F_N \end{bmatrix} + g \begin{bmatrix} \psi_E \\ -\psi_N \end{bmatrix} \tag{2}$$

The first term in Eq. (2) is the *distance*-related error proportional to ψ_A. The second term is the *time*-related error due to the platform tilt ψ_E, ψ_N.

Required Performance of Gyroscopes: By assumptions 4 and 7 for a flight duration of 1 h and subsonic speed, $\dot{\psi}_A = 0.1$ deg/h can be tolerated. $\dot{\psi}_N$ and $\dot{\psi}_E$, however, must not exceed 0.01 deg/h.

In the strapdown mechanization, however, all three angular rate measurements interact to yield the required direction-cosine matrix. Thus, all angular rate measurements must be in the 0.01 deg/h class. The dynamic range of a strapdown gyro for missions characterized in assumptions 1-9 is from 0.01 deg/h to 100 deg/s, i.e., a dynamic range of 36×10^6 as compared to gimballed platforms in which the required dynamic range is 0.01 to 10 deg/h, i.e., 10^3. The resulting intensive torquer activity and greater demands on torquer scale factor accuracy essentially exclude moderate cost spinning wheel gyros for strapdown systems even for the relatively benign mission requiremnts considered here.

Alignment and Calibration: A comparison of the effect of gyro and accelerometer axes alignment error on navigation accuracy for gimballed and strapdown systems is given in Ref. 2. It is indicated that levelling in the strapdown mechanization is valid only for the airframe orientation on the ground. In subsequent turns during flight, the computer derived axis system tilts with respect to the instrument package. This effect does not exist in gimballed systems. These errors are flight profile dependent and cannot easily be detected on the ground.

Sensitivity to Dynamical Environment: The mechanization of $T_{G/b}$ is determined by gyro measurements, and F_b by the accelerometers. Mechanical vibration of the instrument package may excite correlated signals in $T_{G/b}$ and F_b and

cause a bias in F_G.[3] This susceptibility does not actually exist in the gimballed system.

3. Transformation

In the gimballed mechanization with its coordinate frame (X_p, Y_p, Z_p) perfectly aligned with (X_G, Y_G, Z_G), the transformation of $F_p = [F_{xp}, F_{yp}, F_{zp}]^T$ to F_G is $T_{G/a} = T_{G/p} = I$ and ideally $F_p = F_G$. In view of assumption 2, the mechanization normally requires at least three gimbals. In the strapdown mechanization, the instrumentation axis frame being the A/F body axis (X_b, Y_b, Z_b), $F_b = [F_{xp}, F_{yp}, F_{zp}]^T$, $F_G = T_{G/a} = T_{G/b}$, and $F_G = T_{G/b} F_b$, where $T_{G/b} = [\phi]_x [\theta]_y [\psi]_z$ is the 9-element direction-cosine transformation matrix. *All three* components F_{xb}, F_{yb}, and F_{zb} must be measured to determine F_N, F_E. $T_{G/b}$ is obtained from the differential equation.[3]

$$\dot{T}_{G/b} = -T_{G/b}\Omega_b + \Omega_G T_{G/b} \tag{3}$$

Ω_b consists of elements determined by the three body-axis angular rate measurements p, q, and r. It follows that assumptions 1-9 do not permit savings or simplifications in the strapdown mechanization.

4. Computation

In the gimballed mechanization, computation is essentially the integration of Eq. (1). In the strapdown mechanization, in addition to integrating Eq. (1), Eq. (3) must be integrated and F_G must be computed at the normal iteration rates of 40 Hz. Thus, assumptions 1-9 do not lead to compromises with regard to computational volume and speed. A comparison[2] of a completely coded navigation program of a strapdown system with a program of a gimballed INS shows that the latter uses 30% of the real-time computer capacity and 30% less memory storage than the strapdown system.

5. Rationale for a Hybrid Mechanization

The foregoing explains the limitations of widespread use of INS's for the class of missions considered here. However, subject to the assumptions 1-9, by combining the most essential functions of the gimballed concept (isolation of the levelling gyro) with the least critical function of the strapdown concept (azimuth Euler transformation) into a hybrid mechanization, major savings in cost and complexity can be achieved.

III. Description of the Gyroscopic Navigation System (INS)

A complete qualitative description of the hybrid mechanization and INS integration is given in this section along with definitions of axis systems, and symbols used in the analysis in Secs. IV. and V.

A. Gyroscopic Inertial Measurement Unit (GIMU)

The device, schematically shown in Fig. 1, is comprised of the following elements: 1) a levelling gyroscope (LEG), 2) an azimuth gyroscope (AZG), and 3) a two-axis gimbal system g_i, g_o with its torquers T_x, T_y, and pickoffs P_ϕ, P_θ. LEG and AZG are assumed to be identical and of the strapdown-two-degree-of-freedom type. The gimbal assembly is essentially of the type used in conventional vertical gyroscopes with relatively powerful torquers T_x, T_y low-friction synchro-type pickoffs P_ϕ, P_θ and low-friction bearings b-b'. The outer gimbal g_o is hinged to the aircraft frame AF by means of the bearings b-b' along the longitudinal body axis X_b. LEG and AZG are mounted in the inner gimbal g_i and, together with an optional bob weight W, impart an intentional mass unbalance to the two-axis gimbal system with its center of mass l cm below the suspension point, i.e., the intersection of axes X_{gi} and Y_{gi}. The gimbal axis Z_{gi} tends to align itself with Z_l so that η and ξ tend to zero. The specific force vector F is defined here by F_{xl}, F_{yl}, F_{zl} in the local orthogonal coordinate frame X_l, Y_l, Z_l. X is defined along the projection of X_b on OX_lY_l. F_{xl} and F_{yl} induce the torques F_{xl} and F_{yl} induce the torques lF_{xl} and $l\cos\theta\, F_{yl}$ around Y_{go} and X_{go}, respectively, exciting $\dot{\eta}$ and $\dot{\xi}$ which are sensed by the LEG. The corresponding outputs $\dot{\eta}_m$, $\dot{\xi}_m$ are amplified and integrated in the networks G_y, G_x (detailed in Fig. 2), the outputs of which are applied to the gimbal torquers T_x and T_y, counteracting the torques induced by F_{xl} and F_{yl}. With integral control in G_y, G_x, η and ξ are essentially zero in the steady-state. The outputs of G_y and G_x, denoted by F_{xp} and F_{yp}, respectively, are proportional to F_{xl} and F_{yl}. F_{yp} must be corrected by $(\cos\theta)^{-1}$. F_{zl} does not exert a torque and is not measured. The dynamic range of F_{xp} and F_{yp} is determined by the ratio of the maximum torques available from T_x and T_y to the friction torques T_f in the gimbal bearings. Realistic values of these torques show that a dynamic range of 10^4 can be obtained. The device performs as a two-axis, horizontally stabilized accelerometer independent of vehicle roll ϕ and pitch θ, but dependent on ψ. Assuming $\psi = \psi_0$ before takeoff is known, any subsequent yaw rate $\dot{\psi}$ sensed by AZG is integrated by I_{nx}, and ψ is continuously determined. The pitch θ and roll ϕ measurements, obtained from P_θ and P_ϕ, are insensitive to acceleration and can be used for flight control and display purposes in a conventional manner. Since, in view of Sec. II, the accuracy in $\dot{\psi}$ is ~ 0.1 deg/h, and since $\dot{\psi}_{max} \simeq 10$ deg/s, the dynamic range required from the AZG is only 36×10^4, which is ~ 100 times smaller than in typical strapdown applications. A low-cost gyro can meet this requirement. From Sec. II, the LEG must have a null point stability of 0.01 deg/h. However, this gyro essentially operates in a gimballed mode and its required dynamic range is only 10^4.

B. Integration of the GIMU into a Complete INS

With $F_p = [F_{xp}, F_{yp}]^T$ and ψ provided by the GIMU, the transformation $F_G = T_{G/p} F_p$ reduces to $F_G = [\psi]_z^T F_p$ from which V_G is obtained by integrating Eq. (2), and further integration yields position X_G, Y_G. The following gyro torquer precession commands complete the system as an INS: 1) Schuler tuning—$\dot{\eta}_c^s, \dot{\xi}_c^s$ derived from V_N, V_E and determined in body axes, fed to T_η, T_ξ; 2) Earth rate compensation—$\dot{\eta}_c^\Omega, \dot{\xi}_c^\Omega, \dot{\psi}_c^\Omega$ derived from Ω_s and fed to T_η, T_ξ, T_ψ; 3) compensation of g-dependent gyro drift—derived from

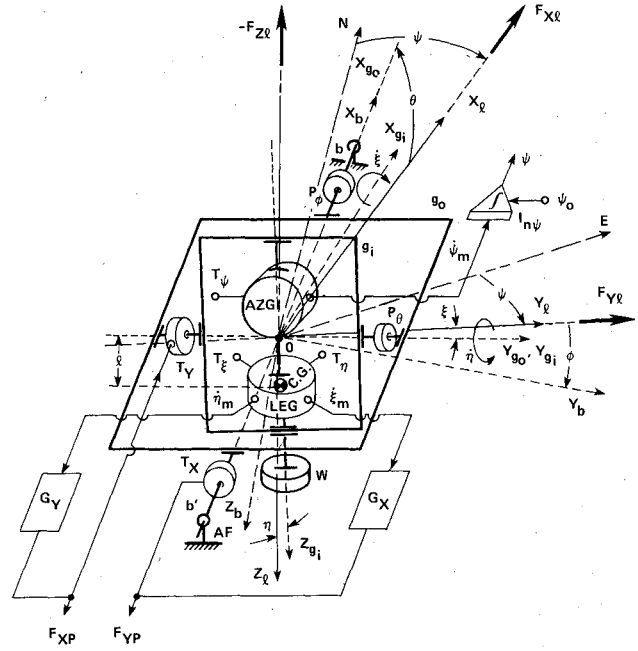

Fig. 1 Description and definition of axis system of the two-gimbal gyro-pendulum and principal loop closures.

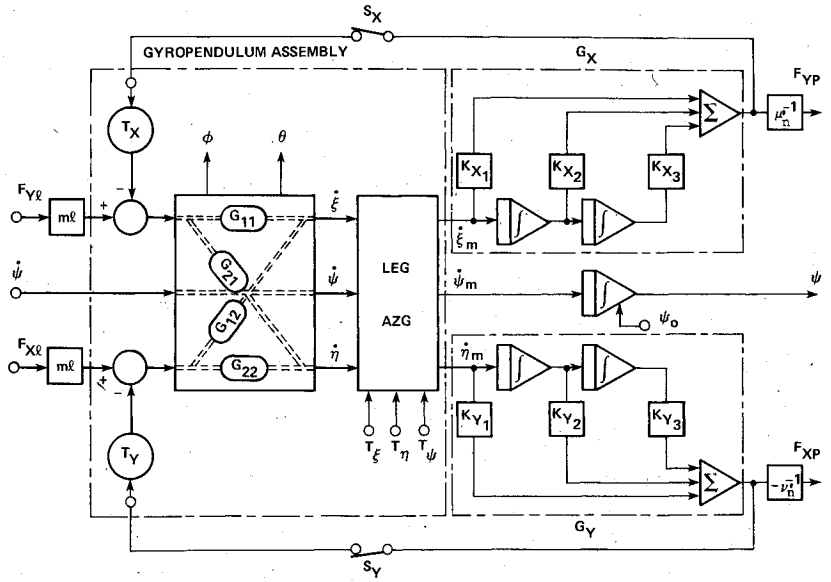

Fig. 2 Block diagram of the GIMU and implementation of its control loops: $\mu_n' = (I_n/b_x)\mu_n$; $\nu_n' = (J_n/b_y)\nu_n$.

known g-sensitivity coefficients of the gyros and from actual values of F_{xp}, F_{yp} and fed to T_η, T_ξ, T_ψ.

IV. Analysis of System Dynamics and Control

In this section, the mathematical model of the gyropendulum assembly shown in Fig. 1 is developed. The resulting equations of motion are then used in the analysis of the closed-loop GIMU.

A. Open-Loop Gyro-Pendulum Dynamics

The LEG and AZG, assumed to be of the two-degree-of freedom (2-DOF) dry tuned rotor (DTR) type are described in detail in Ref. 9. Their open-loop transfer functions are equivalent to those of a classical two-axis symmetrical free rotor gyro given by

$$\theta_x(s) = -\phi_x(s) + \frac{sM_x(s) - M_y(s)(H/I^r)}{I^r s(s^2 + (H/I^r)^2)}$$

$$\theta_y(s) = \phi_y(s) + \frac{M_x(s)(H/I^r) + sM_y(s)}{I^r s(s^2 + (H/I^r)^2)}$$

(x,y,z) is the gyro casing reference frame; ϕ_x and ϕ_y are the angular inputs resolved along x and y; θ_x and θ_y are the angular outputs, i.e., deflection of rotor with respect to gyro case; M_x and M_y are torques applied to rotor resolved along the gyro case coordinate frame; H is the angular momentum of rotor; and I^r is the moment of inertia of rotor about its x and y axes. The loop closure of the gyro is implemented by setting $M_y(s) = A(s)\theta_x(s)$ and $M_x(s) = -A(s)\theta_y(s)$. By proper design of the torquing amplifier $A(s)$, the closed-loop transfer functions are essentially $\theta_x(s) = -(H/A(s))\dot{\phi}_x$ and $\theta_y(s) = -(H/A(s))\dot{\phi}_y$. The development of the equations of motion of the gimbal system is based on Ref. 11. For small values of η and ξ, the equations reduce to

$$I\ddot{\xi} + H\dot{\eta} = -Wl\xi + glF_{yl} \tag{4}$$

$$J\ddot{\eta} - H\dot{\xi} = -Wl\eta - glF_{xl} \tag{5}$$

where $I \triangleq I_x^r + I_x^{gi} + I_x^{go}$, $J \triangleq I_y^r + I_y^{gi}$, $H = I_z^r n$, and $I_y^r = I_x^r = I^r$. Cosθ, friction torques, and reaction torques due to a yaw rate $\dot{\psi}$ of the AZG are disregarded in Eqs. (4) and (5), and are treated as disturbances in Sec. VI. Dividing Eqs. (4) and (5) by I and J, respectively,

$$\ddot{\xi} + a\dot{\eta} = -\mu(g\xi - F_{yl}) \tag{6}$$

$$\ddot{\eta} - b\dot{\xi} = -\nu(g\eta + F_{xl}) \tag{7}$$

where $a \triangleq H/I$, $b \triangleq H/J$, $\mu \triangleq ml/I$, and $\nu \triangleq ml/J$. Laplace transforming of Eqs. (6) and (7) and rearranging, results in

$$[(s^2+\mu g)(s^2+\nu g) + abs^2]\xi = (s^2+\nu g)\mu F_{yl} - as\nu F_{xl} \tag{8}$$

$$[(s^2+\mu g)(s^2+\nu g) + abs^2]\eta = (s^2+\mu g)F_{xl} + bs\mu F_{yl} \tag{9}$$

The characteristic equation is the quartic

$$s^4 + [g(\mu+\nu) + ab]s^2 + \mu\nu g^2 = 0$$

Its solution is

$$s^2 = -\tfrac{1}{2}[g(\mu+\nu) + ab] \pm \{\tfrac{1}{4}[g(\mu+\nu) + ab]^2 - \mu\nu g^2\}^{\frac{1}{2}}$$

It is easily verified that the discriminant is nonnegative so that the two roots are $\omega_1 = \pm js_1$ and $\omega_2 = \pm js_2$.

Equations (8) and (9) indicate an undamped conical oscillation at the two frequencies ω_1 and ω_2. As an example, the following numerical values are assumed: $H = 8$ g-cm-s, $I = 1$ g-cm-s^2, $J = 0.5$ g-cm-s^2, $ml = 0.5$ g-s^2. Thus, $a = 8$ s^{-1}, $b = 16$ s^{-1}, $\mu = 0.5$ cm^{-1}, $\nu = 1$ cm^{-1}, and $g = 981$ cm/s^2, resulting in $\omega_1 = 20.04$ s^{-1} and $\omega_2 = 34.60$ s^{-1}. Expressing Eqs. (8) and (9) in terms of ω_1 and ω_2 and in response to step inputs F_{xl} and F_{yl}, the solutions for $\xi(s)$ and $\eta(s)$ are

$$\xi(s) = \frac{\mu(s^2+\nu g)}{s(s^2+\omega_1^2)(s^2+\omega_2^2)} F_{yl} - \frac{a\nu}{(s^2+\omega_1^2)(s^2+\omega_2^2)} F_{xl} \tag{10}$$

$$\eta(s) = \frac{\nu(s^2+\mu g)}{s(s^2+\omega_1^2)(s^2+\omega_2^2)} F_{xl} + \frac{b\mu}{(s^2+\omega_1^2)(s^2+\omega_2^2)} F_{yl} \tag{11}$$

Equations (10) and (11) show that the sensitivities of ξ and η to F_{yl} and F_{xl} are not equal. In the foregoing analysis of the pendulum dynamics, damping due to friction has been disregarded.

B. Closed-Loop Analysis

The loop closure of the pendulum is schematically described in Fig. 1. Let $\dot{\xi}_d$ and $\dot{\eta}_d$ denote the unknown drift

rates of the LEG, then its outputs are

$$\dot{\xi}_m = \dot{\xi} - \dot{\xi}_d \qquad \dot{\eta}_m = \dot{\eta} - \dot{\eta}_d \tag{12}$$

Considering initial tilt angles ξ_i and η_i, the closed-loop equations are

$$I\ddot{\xi} + H\dot{\eta} = -ml[g(\xi+\xi_i) - F_{yl}] - G_x b_x \dot{\xi}_m \tag{13}$$

$$J\ddot{\eta} - H\dot{\xi} = -ml[g(\eta+\eta_i) + F_{xl}] - G_y b_y \dot{\eta}_m \tag{14}$$

b_x and b_y are the torque coefficients of the gimbal torquers T_x and T_y. In order to implement integral control, G_x and G_y are

$$G_x = K_{x1} + K_{x2}\int dt + K_{x3}\int\int dt'\,dt \tag{15}$$

$$G_y = K_{y1} + K_{y2}\int dt + K_{y3}\int\int dt'\,dt \tag{16}$$

Substituting Eqs. (15), (16), and (12) into Eqs. (13) and (14), dividing through by I and J, respectively, and by Laplace transforming and rearranging, the solutions of $\xi(s)$ and $\eta(s)$ are

$$\xi(s) = \frac{X(s)\Delta_y(s) - s^2 aY(s)}{\Delta_x(s)\Delta_y(s) + abs^4} \tag{17}$$

$$\eta(s) = \frac{Y(s)\Delta_x(s) + s^2 bX(s)}{\Delta_x(s)\Delta_y(s) + abs^4} \tag{18}$$

where

$$X(s) \triangleq s(\mu F_{yl} - \mu g\xi_i) + (A_{x_1}s^2 + A_{x_2}s + A_{x_3})\dot{\xi}_d/s$$

$$Y(s) \triangleq s(-\nu F_{xl} - \nu g\eta_i) + (A_{y_1}s^2 + A_{y_2}s + A_{y_3})\dot{\eta}_d/s$$

$$\Delta_x(s) \triangleq s^3 + A_{x_1}s^2 + (A_{x_2} + \mu g)s + A_{x_3}$$

$$\Delta_y(s) \triangleq s^3 + A_{y_1}s^2 + (A_{y_2} + \nu g)s + A_{y_3}$$

where

$$A_{x_i} \triangleq K_{x_i} b_x / I \qquad A_{y_i} \triangleq K_{y_i} b_y / J \qquad (i = 1,2,3)$$

Since A_{x_i} and A_{y_i} are large compared with a and b, the 6th-order expressions (17) and (18) simplify to

$$\xi(s) = \frac{X(s)}{\Delta_x(s)} = \frac{s\mu(F_{yl} - g\xi_i) + (A_{x_1}s^2 + A_{x_2}s + A_{x_3})\dot{\xi}_d/s}{s^3 + A_{x_1}s^2 + (A_{x_2} + \mu g)s + A_{x_3}} \tag{19}$$

$$\eta(s) = \frac{Y(s)}{\Delta_y(s)} = \frac{-s\nu(F_{xl} + g\eta_i) + (A_{y_1}s^2 + A_{y_2}s + A_{y_3})\dot{\eta}_d/s}{s^3 + A_{y_1}s^2 + (A_{y_2} + \nu g)s + A_{y_3}} \tag{20}$$

Since $\dot{\xi}_d$ and $\dot{\eta}_d$ are assumed to be slow processes, Eqs. (19) and (20) reduce to $\xi(t) = \int\dot{\xi}_d dt$ and $\eta(t) = \int\dot{\eta}_d dt$ in the steady-state ($s \to 0$). That is, the gimbal system tracks the LEG gyro tilt drift angles as expected. The outputs of G_x and G_y, i.e., the torquing signals of T_x and T_y are

$$m_x = G_x\dot{\xi}_m = G_x(\dot{\xi} - \dot{\xi}_d) \tag{21}$$

$$m_y = G_y\dot{\eta}_m = G_y(\dot{\eta} - \dot{\eta}_d) \tag{22}$$

By differentiating $\xi(s)$ and $\eta(s)$ in Eqs. (19) and (20), substituting into Eqs. (21) and (22), rearranging and substituting K_{xi} and K_{yi} by $A_{xi}b_x/I$ and $A_{yi}b_y/J$, the results are

$$m_x = \frac{I}{b_x}\frac{A_{x_1}s^2 + A_{x_2}s + A_{x_3}}{s^3 + A_{x_1}s^2 + (A_{x_2} + \mu g)s + A_{x_3}} \times [\mu F_{yl} - \mu g\xi_i - \mu g\dot{\xi}_d/s - s\dot{\xi}_d] \tag{23}$$

$$m_y = \frac{J}{b_y}\frac{A_{y_1}s^2 + A_{y_2} + A_{y_3}}{s^3 + A_{y_1}s^2 + (A_{y_2} + \nu g)s + A_{y_3}} \times [-\nu F_{xl} - \nu g\eta_i - \nu g\dot{\eta}_d/s - s\dot{\eta}_d] \tag{24}$$

With knowledge of the nominal values I_n, J_n, b_{xn}, and b_{yn}, the measured specific forces F_{yp} and F_{xp} for $s \to 0$ are defined by $F_{yp} = m_x b_{xn}/I_n\mu_n$ and $F_{xp} = m_y b_{yn}/J_n(-\nu_n)$. Specifically,

$$F_{yp} = \beta_y(F_{yl} - g\xi_i - g\dot{\xi}_d/s) \tag{25}$$

$$F_{xp} = \beta_x(F_{xl} + g\eta_i + g\dot{\eta}_d/s) \tag{26}$$

The coefficients $\beta_y = (I\mu/b_x)(b_{xn}/I_n\mu_n)$ and $\beta_x = -(J\nu/b_y) \times (b_{yn}/J_n\nu_n)$ ideally are equal to unity. In view of Sec. III, β_y must be divided by $\cos\theta$.

Thus, the closed-loop system is equivalent to two orthogonal accelerometers mounted on a platform with the initial tilt errors ξ_i and η_i and the corresponding tilt drift errors $\dot{\xi}_d/s$ and $\dot{\eta}_d/s$. Its unique property is that accelerometer bias or alignment errors are nonexisting since the instrumentation error stems from the single source $\dot{\xi}_d, \dot{\eta}_d$. The effect of gimbal bearing friction and torquer hysteresis is discussed in Sec. VI.

Typical values for A_{x1}, A_{x2}, and A_{x3} yielding closed-loop poles at $\omega_{1,2} = -30 \pm 30j$ and $\omega_3 = -40$ for $\mu g = 0.5 \times 981 = 490$ are: $A_{x1} = 100$, $A_{x2} = 2810$, $A_{x3} = 36{,}000$. Similarly, for the same closed-loop poles, for $\nu g = 1 \times 981$: $A_{y1} = 100$, $A_{y2} = 2320$, and $A_{y3} = 36{,}000$. These values thus provide a bandwidth of ~ 5 Hz, which is adequate for the acceleration inputs in typical flight missions. The effect of possible high-frequency vibrations is discussed in Sec. VI.

A block diagram describing the closed-loop system is shown in Fig. 2. In it $G_{11}(s)$, $G_{12}(s)$, $G_{21}(s)$, and $G_{22}(s)$, as derived from Eqs. (10) and (11), are defined by

$$\dot{\xi}(s) = \frac{\mu s(s^2 + \nu g)}{(s^2 + \omega_1^2)(s^2 + \omega_2^2)}F_{yl} - \frac{a\nu s^2}{(s^2 + \omega_1^2)(s^2 + \omega_2^2)}F_{xl} \tag{27}$$

$$\dot{\eta}(s) = -\frac{\nu s(s^2 + \mu g)}{(s^2 + \omega_1^2)(s^2 + \omega_2^2)}F_{xl} + \frac{b\mu s^2}{(s^2 + \omega_1^2)(s^2 + \omega_2^2)}F_{yl} \tag{28}$$

The switches S_x and S_y in the torquing loops will be referred to in Sec. V.

V. Schuler Tuning, Gyrocompassing, and Calibration

A. Implementation of Schuler Tuning

Schuler tuning is assured by applying the required precession commands $\dot{\xi}_c^s$ and $\dot{\eta}_c^s$ to the torquers T_ξ and T_η of the LEG. These commands are obtained from $\dot{\xi}_E = V_E/R$ and $\dot{\eta}_N = -V_N/R$, respectively, where V_E and V_N are determined by the solution of Eq. (1). $\dot{\xi}_c^s$ and $\dot{\eta}_c^s$ must be implemented in the X_l, Y_l, Z_l coordinate frame. The corresponding transformed components are

$$\begin{bmatrix} \dot{\eta}^s \\ \dot{\xi}^s \end{bmatrix} = [\psi]^T \begin{bmatrix} -V_N/R \\ V_E/R \end{bmatrix} \tag{29}$$

By setting $\dot{\eta}_c^s = \dot{\eta}^s$ and $\dot{\xi}_c^s = \dot{\xi}^s$, the required precession is implemented. For the class of missions considered here (short time and moderate speed), defined in Sec. II, the analysis of the Schuler tuning can be based on the approximation that the second term on the right-hand side of Eq. (1) is negligible,[11] i.e.,

$$\dot{V}_N \simeq F_N \qquad \dot{V}_E \simeq F_E \tag{30}$$

Thus, the small amplitude components at the sidereal frequency Ω_s are disregarded. V_N and V_E are obtained by integrating Eq. (1). In accordance with Eq. (2), the tilt angles η^0 and ξ^0 are substituted for ψ_E and ψ_N in the X_l, Y_l, Z_l frame so that the measured specific forces F_{xp} and F_{yp} are

$$F_{xp} = F_{xl} + g\eta^0 \tag{31}$$

$$F_{yp} = F_{yl} - g\xi^0 \tag{32}$$

where, in accordance with Eqs. (25) and (26),

$$\eta^0 \triangleq \eta_i + \dot{\eta}_d/s \tag{33}$$

$$\xi^0 \triangleq \xi_i + \dot{\xi}_d/s \tag{34}$$

It is assumed here that $\beta_x = \beta_y = 1$.

From Eqs. (29) and (30), the required precession rates in the X_l, Y_l, Z_l axis frame are

$$\begin{bmatrix} \dot{\eta}^s \\ \dot{\xi}^s \end{bmatrix} = \frac{1}{R}[\psi]^T \int [\psi]^T \begin{bmatrix} F_{xp} \\ F_{yp} \end{bmatrix} dt \tag{35}$$

The analysis of Eq. (35) must be performed in geographical coordinates, namely

$$\begin{bmatrix} -\dot{\eta}_N \\ \dot{\xi}_E \end{bmatrix} = \frac{1}{R} \int [\psi]^T \begin{bmatrix} F_{xp} \\ F_{yp} \end{bmatrix} dt \tag{36}$$

With torquing commands applied to T_ξ and T_η, F_{yp} and F_{xp} are determined with respect to the rotating local vertical, i.e.,

$$F_{xp} = F_{xl} + g\eta^0 + g(\eta - \dot{\eta}_c^s/s) \tag{37}$$

$$F_{yp} = F_{yl} - g\xi^0 - g(\xi - \dot{\xi}_c^s/s) \tag{38}$$

Substituting Eqs. (37) and (38) into Eq. (36), performing the Euler transformation, and since $\dot{\eta}_N = -V_N/R$ and $\dot{\xi}_E = V_E/R$, we have

$$-\dot{\eta}_N = \frac{1}{R}\left[\int F_N dt + g\int \eta_N^0 dt + g\int \eta_N dt + g\int\int \frac{V_N}{R} dt'\, dt\right] \tag{39}$$

$$\dot{\xi}_E = \frac{1}{R}\left[\int F_E dt - g\int \xi_E^0 dt - g\int \xi_E dt + g\int\int \frac{V_E}{R} dt'\, dt\right] \tag{40}$$

In the last expression, the small angles ξ and η (dropping indices) are treated as vectors so that

$$\eta_N = \eta\cos\psi + \xi\sin\psi \qquad -\xi_E = -\eta\sin\psi + \xi\cos\psi \tag{41}$$

By Laplace transforming and rearranging Eqs. (39) and (40), we have, in view of the approximation (30),

$$s\eta_N = -\frac{V_N}{R} - \frac{g}{Rs}\eta_N^0 - \frac{g}{Rs}\eta_N - \frac{g}{R^2}\frac{V_N}{s^2} \tag{42}$$

$$s\xi_E = \frac{V_E}{R} - \frac{g}{Rs}\xi_E^0 - \frac{g}{Rs}\xi_E + \frac{g}{R^2}\frac{V_E}{s^2} \tag{43}$$

With $g/R = \omega_s^2$, the solutions for η_N and ξ_E are

$$\eta_N(s) = -\frac{\omega_s^2}{s^2 + \omega_s^2}\eta_N^0 - \frac{V_N}{Rs} \tag{44}$$

$$\xi_E(s) = -\frac{\omega_s^2}{s^2 + \omega_s^2}\xi_E^0 + \frac{V_E}{Rs} \tag{45}$$

Equations (44) and (45) reveal the familiar sinusoidal Schuler frequency oscillation due to η_N^0 and ξ_N^0, and the rotation resulting from vehicular velocities V_N and V_E. η_N^0 and ξ_E^0 are functions of ψ since they originate from errors in the X_l and Y_l axes. Thus, changes in ψ during flight "modulate" the random process $\dot{\xi}_d, \dot{\eta}_d$ so that the error propagation also depends on the actual flight path. The actual specific force F_N, F_E in geographical coordinates is obtained by transforming Eqs. (37) and (38) into geographical coordinates,

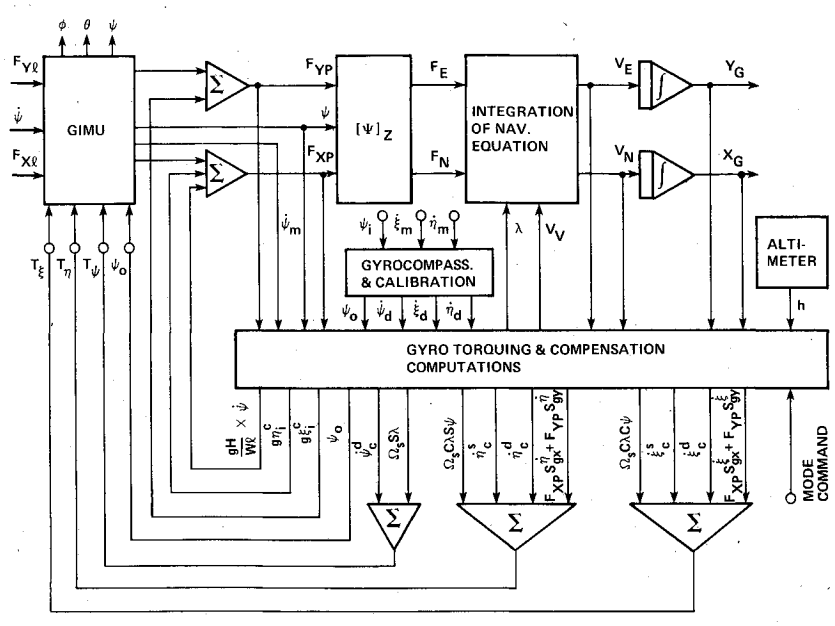

Fig. 3 Integration of the GIMU in a complete inertial measurement system.

using Eq. (30), and substituting Eqs. (44) and (45)

$$F_N = \dot{V}_N + g\eta_N^0 + g\left[-\frac{\omega_s^2}{s^2+\omega_s^2}\eta_N^0 - \frac{V_N}{Rs} + \frac{V_N}{Rs}\right]$$

$$= \dot{V}_N + g\frac{s^2}{s^2+\omega_s^2}\eta_N^0 \tag{46}$$

$$F_E = \dot{V}_E - g\xi_E^0 - g\left[-\frac{\omega_s^2}{s^2+\omega_s^2}\xi_E^0 + \frac{V_E}{Rs} - \frac{V_E}{Rs}\right]$$

$$= \dot{V}_E - g\frac{s^2}{s^2+\omega_s^2}\xi_E^0 \tag{47}$$

The description of the Schuler tuning implementation is incorporated in Fig. 3.

B. Gyrocompassing

The mass unbalance of the gyro-pendulum can be advantageously used to achieve rapid gyrocompassing. On the ground, with switches S_x and S_y in Fig. 2 open, the pendulum theoretically aligns itself with the local vertical. The deviation from the true vertical is determined by two factors: 1) the friction torques of the gimbal bearings, and 2) the reaction torques of the gyros due to Ω_s.

1) Assuming a bearing friction torque of $T_f = 0.2$ g-cm and a mass unbalance of $Wl = 800$ g-cm, the deviation $\Delta\xi$ or $\Delta\eta$ is $T_f/wl = 0.2/800 = 250\,\mu$ rad.

2) The reaction torques exerted on the gimbal system by the LEG and AZG due to the Earth components $\Omega_s\cos\lambda$ and $\Omega_s\sin\lambda$, respectively, are nearly equal at moderate latitudes $\lambda \sim 45$ deg, and amount to ~ 10 deg/h. For an angular momentum of the gyros $H = 8$ g-cm s, the total reaction torque is $(2\times 8\times 10)/(3600\times 57.3) = 8\times 10^{-4}$ g-cm. This is negligible in comparison with the friction torque and can be disregarded. The requirement for precision in azimuth measurement is determined as follows. At the heading angle ψ, the Earth rate components in the X_l, Y_l, Z_l frame are

$$\begin{bmatrix} \cos\psi & \sin\psi & 0 \\ -\sin\psi & \cos\psi & 0 \\ 0 & 0 & 1 \end{bmatrix} \begin{bmatrix} \Omega_s\cos\lambda \\ 0 \\ \Omega_s\sin\lambda \end{bmatrix} = \begin{bmatrix} \cos\psi\Omega_s\cos\lambda \\ -\sin\psi\Omega_s\cos\lambda \\ \Omega_s\sin\lambda \end{bmatrix} \tag{48}$$

As a result of the orientation error vector $[\Delta\xi, \Delta\eta, \Delta\psi]^T$, the error vector in sensing Earth rate $[\delta\dot{\xi}_E, \delta\dot{\eta}_E, \delta\dot{\psi}_E]^T$ is given by

$$\begin{bmatrix} \delta\dot{\xi}_E \\ \delta\dot{\eta}_E \\ \delta\dot{\psi}_E \end{bmatrix} = \begin{bmatrix} 0 & \Delta\psi & -\Delta\eta \\ -\Delta\psi & 0 & \Delta\xi \\ \Delta\eta & -\Delta\xi & 0 \end{bmatrix} \begin{bmatrix} \cos\psi\Omega_s\cos\lambda \\ -\sin\psi\Omega_s\cos\lambda \\ \Omega_s\sin\lambda \end{bmatrix}$$

$$= \begin{bmatrix} -\Delta\psi\sin\psi\Omega_s\cos\lambda - \Delta\eta\Omega_s\sin\lambda \\ -\Delta\psi\cos\psi\Omega_s\cos\lambda + \Delta\xi\Omega_s\sin\lambda \\ \Delta\eta\cos\psi\Omega_s\cos\lambda + \Delta\xi\sin\psi\Omega_s\cos\lambda \end{bmatrix} \tag{49}$$

Since $\Delta\xi$ and $\Delta\eta$ are $\sim 250\mu$ rad and $\Omega_s\cos\lambda$ is ~ 10 deg/h, the elements multiplying $\Delta\eta$ or $\Delta\xi$ are in the order of 0.0025 deg/h or less and can be neglected. The remaining terms are essentially: $\Delta\dot{\xi} = -\Delta\psi\sin\psi\Omega_s\cos\lambda$, $\Delta\dot{\eta} = -\Delta\psi\cos\psi\Omega_s\cos\lambda$, and $\dot{\psi} \simeq 0$. The largest tolerable errors $\delta\dot{\xi}_E$ and $\delta\dot{\eta}_E$ in the 1 n.mi./h class are 0.01 deg/h. Thus, $\Delta\psi = 0.01$ deg/h/10 deg/h $= 0.001$ rad $= 0.057$ deg. Therefore, gyrocompassing must be accomplished with a precision of at least 0.057 deg.

The longitudinal aircraft axis on the ground deviates from the geographical north by the unknown angle ψ. The measured rate outputs of the LEG are then

$$\begin{bmatrix} \dot{\xi}_m \\ \dot{\eta}_m \end{bmatrix} = \begin{bmatrix} \cos\psi & \sin\psi \\ -\sin\psi & \cos\psi \end{bmatrix} \begin{bmatrix} \Omega_s\cos\lambda \\ 0 \end{bmatrix} - \begin{bmatrix} \dot{\xi}_d \\ \dot{\eta}_d \end{bmatrix}$$

$$= \begin{bmatrix} \cos\psi \\ -\sin\psi \end{bmatrix} \Omega_s\cos\lambda - \begin{bmatrix} \dot{\xi}_d \\ \dot{\eta}_d \end{bmatrix} \tag{50}$$

$\dot{\xi}_m$ and $\dot{\eta}_m$ are fed to a resolver with a variable input angle ψ_i, as indicated in Fig. 3. The resolved outputs $\dot{\xi}_R$ and $\dot{\eta}_R$ are

$$\begin{bmatrix} \dot{\xi}_R \\ \dot{\eta}_R \end{bmatrix} =$$

$$\begin{bmatrix} \cos(\psi-\psi_i) - (\dot{\xi}_d/\Omega_s\cos\lambda)\cos\psi_i + (\dot{\eta}_d/\Omega_s\cos\lambda)\sin\psi_i \\ -\sin(\psi-\psi_i) - (\dot{\eta}_d/\Omega_s\cos\lambda)\cos\psi_i - (\dot{\xi}_d/\Omega_s\cos\lambda)\sin\psi_i \end{bmatrix} \Omega_s\cos\lambda \tag{51}$$

ψ_i is varied until $\dot{\eta}_R = 0$, so that

$$\sin(\psi-\psi_i) \simeq \psi - \psi_i \triangleq \Delta\psi$$

$$= -(\dot{\xi}_d/\Omega_s\cos\lambda)\sin\psi_i - (\dot{\eta}_d/\Omega_s\cos\lambda)\cos\psi_i \tag{52}$$

Denoting

$$\dot{\xi}_d/\Omega_s\cos\lambda \triangleq a \qquad \dot{\eta}_d/\Omega_s\cos\lambda \triangleq b$$

$$a/(a^2+b^2)^{1/2} \triangleq \cos\alpha \qquad b/(a^2+b^2)^{1/2} \triangleq \sin\alpha$$

we have

$$\sin(\psi-\psi_i) = -\sin(\psi_i+\alpha)(a^2+b^2)^{1/2} = \Delta\psi \tag{53}$$

It is easily verified that for drift rates $\dot{\xi}_d$ and $\dot{\eta}_d$ in the order of 0.02 deg/h, $|\Delta\psi|$ exceeds the limitation of 0.057 deg.

The first row in Eq. (51) can, however, be used to determine $\Delta\psi$, i.e.,

$$\dot{\xi}_R = [\cos(\psi-\psi_i) - a\cos\psi_i + b\sin\psi_i]\Omega_s\cos\lambda \tag{54}$$

If, for example, $\psi - \psi_i = 0.2$ deg, and since $\cos(0.2\text{ deg}) \simeq 1$, by subtracting $\Omega_s\cos\lambda$, the remaining term in Eq. (54) is, after normalization by $\Omega_s\cos\lambda$,

$$e = (\dot{\xi}_R - \Omega_s\cos\lambda)/\Omega_s\cos\lambda = -a\cos\psi_i + b\sin\psi_i \tag{55}$$

Using the same notations as earlier, we have

$$e = -(\cos\alpha\cos\psi_i - \sin\alpha\sin\psi_i)(a^2+b^2)^{1/2} \tag{56}$$

By causing a perturbation $\delta\psi_i$ on ψ_i (e.g., a sine wave of known amplitude), we have

$$\delta e = (\cos\alpha\sin\psi_i + \sin\alpha\cos\psi_i)(a^2+b^2)^{1/2}\delta\psi_i \tag{57}$$

But, from Eq. (53), it follows that $\delta e = \Delta\psi\delta\psi_i$ and

$$\Delta\psi = \delta e/\delta\psi_i \tag{58}$$

$\Delta\psi$ thus determined is added to the value of ψ_i, which nulls $\dot{\eta}_R$ in accordance with Eq. (58). The new value $\psi_i + \Delta\psi = \psi_i^*$ is now applied to the resolver which yields

$$\begin{bmatrix} \dot{\xi}_R^* \\ \dot{\eta}_R^* \end{bmatrix} = \begin{bmatrix} \cos(\psi-\psi_i^*) - a\cos\psi_i^* + b\sin\psi_i^* \\ -\sin(\psi-\psi_i^*) - b\cos\psi_i^* - a\sin\psi_i^* \end{bmatrix} \Omega_s\cos\lambda \tag{59}$$

But, $\psi-\psi_i^*=\psi-\psi_i-\Delta\psi=0$.

Rearranging and subtracting $\Omega_s\cos\lambda$ in the first row, we have

$$\dot{\xi}_R^*-\Omega_s\cos\lambda=-\cos\psi_i^*\dot{\xi}_d+\sin\psi_i^*\dot{\eta}_d \tag{60}$$

$$\dot{\eta}_R^*=-\sin\psi_i^*\dot{\xi}_d-\cos\psi_i^*\dot{\eta}_d \tag{61}$$

From the last two equations, the drift rates are readily determined from

$$\begin{bmatrix}\dot{\xi}_d\\ \dot{\eta}_d\end{bmatrix}=-\begin{bmatrix}\cos\psi_i^* & \sin\psi_i^*\\ -\sin\psi_i^* & \cos\psi_i^*\end{bmatrix}\begin{bmatrix}\dot{\xi}_R^*-\Omega_s\cos\lambda\\ \dot{\eta}_R^*\end{bmatrix} \tag{62}$$

The procedures of gyrocompassing, i.e., Eqs. (51), (58), and calibration (62), provide the appropriate torquing commands $\dot{\xi}_c^d$ and $\dot{\eta}_c^d$ to the LEG. The initial gyrocompassing step defined in Eqs. (51) and (52) is now repeated with $\Delta\psi$ essentially zero, and the Earth rate components $\dot{\eta}_c^\Omega=\Omega_s\cos\lambda\sin\psi_i^*$ and $\dot{\xi}_c^\Omega=\Omega_s\cos\lambda\cos\psi_i^*$ are applied to T_η, T_ξ and S_x, S_y are simultaneously closed. The AZG is subjected to $\Omega_s\sin\lambda$; its output is $\dot{\psi}_{m_z}=\Omega_s\sin\lambda-\dot{\psi}_d$. By subtracting $\Omega_s\sin\lambda$, $\dot{\psi}_d$ is determined and $\dot{\psi}_c^d$ is applied to T_ψ. Bias terms $g\xi_i$ and $g\eta_i$ [Eqs. (25) and (26)], due to possible initial offsets, can be easily eliminated. All the compensation commands are indicated in Fig. 3.

VI. Error Analysis and Evaluation

As shown in Sec. II, the errors originate primarily in angular drift rates of the LEG and AZG gyroscopes which, for a given type of gyroscope, are essentially determined by temperature variations and g-loading. Other error sources originate in uncompensated disturbances due to friction torque, hysteresis, torquer scale factor errors, gyrocompassing, and alignment errors. In the analysis, x denotes position deviation either in the north or east direction.

A. Positional Error Propagation Due to Random Gyro Drift Rate

The specific force measurement error in a Schuler tuned system is given in Eqs. (46) and (47) ξ_E^o and η_N^o, which are angular deviations from the local vertical, consist of constant and random terms as indicated in Eqs. (33) and (34). The following uniform notation is used for drift rates $\dot{\xi}_d$ or $\dot{\eta}_d$ contributing to ξ_E^o and η_N^o:

d = gyro angular drift rate defined in goegraphical coordinates, rad/h

ω_s = Schuler frequency, rad/h

R = distance of vehicle from center of the Earth, m

a^{-1} = correlation time of gyro drift rate process, h

$\alpha\triangleq a/\omega_s$

$\zeta\triangleq\omega_s t$

The drift rate is modelled as a first-order Markov process with the autocorrelation function

$$\phi_{dd}(\tau)=\sigma_d^2 e^{-a|\tau|} \tag{63}$$

where $\sigma_d^2\triangleq\mathrm{Var}(d)$. In time domain, $\mathrm{Var}(x)=\sigma_x^2$ is given by

$$\sigma_x^2=\int_0^t\int_0^t h_x(\tau')h_x(\tau'')\phi_{dd}(\tau'-\tau'')\,d\tau'\,d\tau'' \tag{64}$$

where the impulse response $h_x(t)$, corresponding to $H_x(s)=1/s(s^2+\omega_s^2)$, is $h_x(t)=(1-\cos\omega_s t)/\omega_s^2$. Substituting Eq. (63) and $h_x(t)$ into Eq. (64), and dividing by $\sigma_d^2 g^2$, the normalized double convolution yields

$$\begin{aligned}I=&\frac{1}{\alpha^2(\alpha^2+1)^2}\{\alpha\zeta(3\alpha^2+2)(\alpha^2+1)\\&+2(1-e^{-\alpha\zeta})(\alpha^2+1)[\alpha(\alpha\cos\zeta-\sin\zeta)-1]\\&+2\alpha^3e^{-\alpha\zeta}(\alpha\cos\zeta-\sin\zeta)-\alpha^3(\alpha^2+1)(4\sin\zeta-\tfrac{1}{4}\sin2\zeta)\\&-\alpha^2[\alpha^2+\alpha^2\cos^2\zeta-\sin^2\zeta]\}\end{aligned} \tag{65}$$

Defining $u=(I)^{1/2}$, the standard deviation of x, σ_x is

$$\sigma_x=(R\sigma_d/\omega_s)u \tag{66}$$

Plots of $u(\alpha,\zeta)$ are shown in Fig. 4.

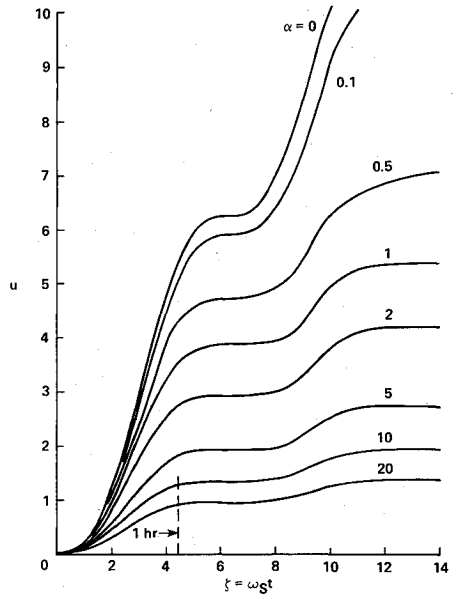

Fig. 4 Normalized positional error propagation as a function of normalized time $\zeta=\omega_s t$ with gyro noise bandwidth $a=\alpha\omega_s$ as a parameter.

B. Velocity Error Propagation Due to Random Gyro Drift Rate

Using the same notations and definitions as in subsection A, the variance of the velocity error v is given by

$$\sigma_v^2=\int_0^t\int_0^t h_v(\tau')h_v(\tau'')\phi_{dd}(\tau'-\tau'')\,d\tau'\,d\tau'' \tag{67}$$

$h_v(t)$, corresponding to $H_v(s)=1/\omega_s^2+s^2)$, is $h_v(t)=\sin\omega_s t/\omega_s$. Substituting Eq. (63) and $h_v(t)$ into Eq. (67), and dividing by $\sigma_d^2 g^2$, the normalized double convolution integral I is

$$\begin{aligned}I=&\frac{1}{(\alpha^2+1)^2}\{\alpha(\alpha^2+1)(\zeta-\tfrac{1}{2}\sin2\zeta)-(\alpha^2\sin^2\zeta-\cos^2\zeta)\\&-2(\alpha^2\sin\zeta+\cos\zeta)e^{-\alpha\xi}+1\}\end{aligned} \tag{68}$$

Defining $u\triangleq(I)^{1/2}$, the standard deviation of v, σ_v is

$$\sigma_v=R\sigma_d u \tag{69}$$

Plots of $u(\zeta,\alpha)$ are shown in Fig. 5.

C. Positional Error Propagation Due to Random Acceleration Error

Using the same notations and definitions as in subsections A and B, and denoting the acceleration error by $g\epsilon$, where ϵ is an equivalent tilt angle from the local vertical, it is clear that

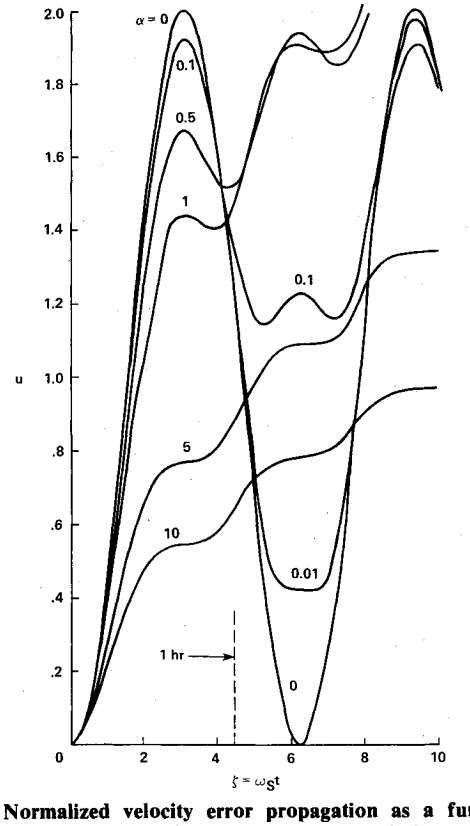

Fig. 5 Normalized velocity error propagation as a function of normalized time $\zeta=\omega_s t$ with gyro noise bandwidth $a=\alpha\omega_s$ as a parameter, or normalized position error due to accelerometer noise with $a=\alpha\omega_s$ as a parameter.

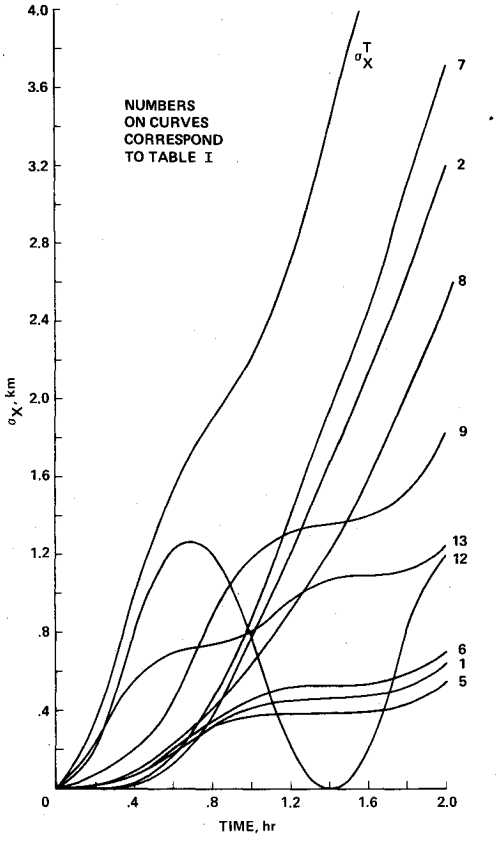

Fig. 6 Positional error propagation with a 100-μ rad initial tilt error, a constant drift rate of the AZG of $\dot{\psi}_d=0.1$ deg/h, and a constant temperature slope of the LEG of 0.5°F/h.

the spectrum of the positional deviation x has the same form as v. Consequently, the standard deviation of x, σ_x is

$$\sigma_x = R\sigma_\epsilon u \tag{70}$$

and u is shown in Fig. 5.

D. Positional Error Propagation Due to Constant Heading Drift Rate Error

From Eq. (49), the uncertainty in determining the Earth rate compensating precession command is $\Delta\dot{\eta}=\Delta\psi\Omega_s\cos\lambda$. Assuming perfect gyrocompassing, i.e., a precise initial value for ψ_0, and a constant unknown azimuth gyro drift rate $\dot{\psi}_d$, $\Delta\psi=\dot{\psi}_d t$, and the equivalent drift rate due to this compensation error is

$$c=\dot{\psi}_d\Omega\cos\lambda \tag{71}$$

The positional divergence σ_x due to this error, in accordance with Eqs. (46) and (47), is $\sigma_x=g\sigma_c/s^3(\omega_s^2+s^2)$. In time domain, $\sigma_x=g\sigma_c[\cos\omega_s t-1)/\omega_s^4+t^2/2\omega_s^2]$. Defining

$$u\triangleq \tfrac{1}{2}\zeta^2-(1-\cos\zeta) \tag{72}$$

σ_x is given by

$$\sigma_x=(R\sigma_c/\omega_s^2)u \tag{73}$$

E. Positional Error Due to a Drift Rate Impulse

A sustained acceleration, e.g., as a result of a turn, can excite a gyro drift rate for the duration of the turn τ. If $\omega_s\tau\ll 1$, this drift rate can be considered as an acceleration impulse $(gd)\tau$. In accordance with Eqs. (46) and (47), it excites a position error

$$\Delta x=(Rd)\tau(1-\cos\zeta) \tag{74}$$

F. Positional Error Due to an Acceleration Impulse

In a turn, $\dot{\psi}$ excites a reaction torque $H\psi$ in the AZG which, for the pendulosity Wl, causes an acceleration error $g\epsilon_r$, where $\epsilon_r=H\dot{\psi}/Wl$. If $\dot{\psi}$ persists for τ s and if $\omega_s\tau\ll 1$, $g\epsilon_r\tau=\Delta v$ is a velocity impulse, causing a position error in accordance with Eqs. (46) and (47)

$$\Delta x=R\omega_s\tau\epsilon_r\sin\zeta \tag{75}$$

G. Friction and Hysteresis Disturbances

Friction torque T_f on the gimbal axis causes zero mean acceleration noise modelled as a binary process $\epsilon_f=\pm T_f/Wl$ with a zero crossing rate a, determined by the airplane pitch and roll motions. Its autocorrelation function is [13]

$$\phi_{\epsilon_f}(\tau)=\epsilon_f^2 e^{-2a|\tau|} \tag{76}$$

From Eqs. (68), (69), and Fig. 5, the effect of a slow rate $a=0.01$ 1/s is given in Table 1. The dead space due to friction $\Delta_f=g\epsilon_f\simeq 250$ μg can be substantially reduced by a torque dither resulting from either a small oscillation or a forced dither command. Torquer hysteresis, being about 0.3% of full scale, may amount to 3 mg. Its effect, due to low-frequency acceleration inputs, causes acceleration noise similar to T_f and is also substantially reduced by the torque dither. The experimental results in Ref. 6, in which torque motors are employed in a similar manner, support the foregoing qualitative assessment of the effects of gimbal torquer nonlinearities.

H. Initial Tilt Error

From Eqs. (46) and (47), the effect of initial tilt error ξ_i, η_i, denoted here by ϵ_i, results in a positional error

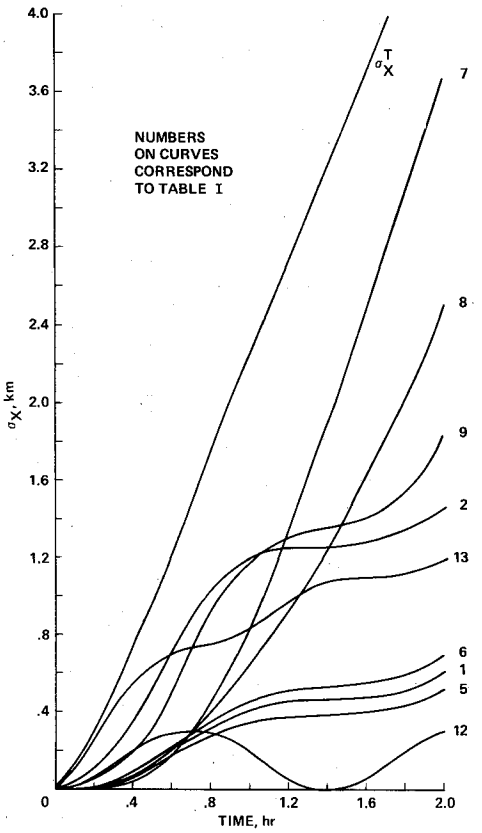

Fig. 7 Positional error propagation with a 25-μ rad initial tilt error, a constant drift rate of the AZG of $\psi_d = 0.1$ deg/h, and a stationary random temperature variation of the LEG of 1°F.

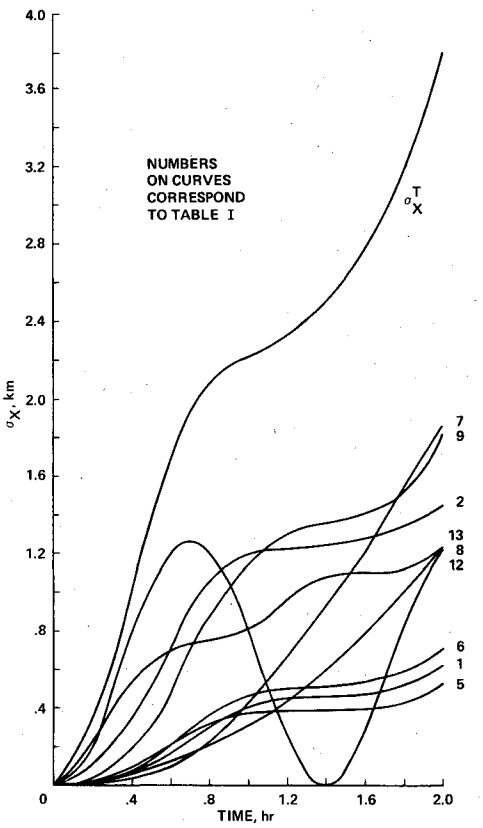

Fig. 8 Positional error propagtion with a 100-μ rad initial tilt error, a drift rate of the AZG of $\psi_d = 0.05$ deg/h, and a stationary random temperature variation of the LEG of 1°F.

Table 1 Positional errors after 1 h of flight

Description of error source	Numerical value	Formula for σ_x and Eq. no.		Comments	σ_x, m at 1 h
1. Non-g-sensitive drift of LEG	0.003 deg/h[a]	$R\sigma_d u/\omega_s$	(66)	d = const, calibration compensated to 0.1 d; $\alpha = 0$	403*
2. Drift of LEG due to temperature variation	0.03 deg/h/°F[a]	$R\sigma_c u/\omega_s^2$	(73)	Constant slope of 0.5°F/h	754*
3. g-sensitive drift of LEG due to turbulence	0.05 deg/h/g[a]	$R\sigma_d u/\omega_s$	(66)	0.25 g rms input; $\alpha = 2$ compensated to ~5%	(1685) 85
4. g-sensitive drift of LEG due to turn or deceleration	0.05 deg/h/g[a]	$R\mathrm{d}\tau(1-\cos\zeta)$	(74)	Duration $\tau = 100$ s error compensated to ~5%	(150)
5. Random drift in LEG	0.005 deg/h[a]	$R\sigma_d u/\omega_s$	(66)	Correlation time $a^{-1} = 0.15$ h; $\alpha = a/\omega_s = 1.5$	387*
6. Torquer scale factor error of LEG	$\epsilon_T = 0.003$[a]	$R\sigma_d u/\omega_s$	(66)	Equivalent to drift rate $d = \epsilon_T V/R$; $V = 200$ m/s	453*
7. Error in Earth rate computation due to $\dot{\psi}_d$ in AZG	0.1 deg/h[b]	$R\sigma_c u/\omega_s^2$	(73)	AZG subjected to ~10 deg/s, thus larger drift rate $\dot{\psi}_d$	874*
8. Error in azimuth transformation due to $\dot{\psi}_d$ in AZG	0.1 deg/h[b]	$\iint v\dot{\psi}_d \mathrm{d}t'\,\mathrm{d}t$		V is assumed to be 200 m/s	628*
9. Gyrocompassing error	$\Delta\psi = 0.05$ deg	$R\sigma_d u/\omega_s$	(66)	Equivalent to $d = 0.0087$ deg/h at latitude $\lambda \simeq 45$ deg	1172*
10. Reaction torque of AZG due to sutained $\dot{\psi} = 0.1$ rad/s for $\tau = 100$	$\epsilon_r = 4$ mR, based on $H = 8$ g-cm-s	$R\omega_s\tau\epsilon_r\sin\zeta$	(75)	Equivalent to acceleration angle $\epsilon_r = H\dot{\psi}/Wl = 0.1 \times 8 \times 800$; 0.001 compensated to ~1%	800 8
11. Reaction torque of AZG due to $\dot{\psi} = 0.1$ rad/s rms excited by turbulence	$\epsilon_r = 4$ mR, based on $H = 8$ g-cm-s	$R\sigma_\epsilon u$	(70)	Bandwidth of $\dot{\psi}$ $a = 0.5$ rad/s; $\alpha = a/\omega_s = 6.7$; compensated to ~1%	(23,000) 230
12. Initial tilt error	$\epsilon_i = 100\ \mu$rad	$R\epsilon_i(1-\cos\zeta)$	(77)	100μ rad is assumed feasible	797*
13. Acceleration noise due to to bearing friction	$\epsilon_f = T_f/Wl$	$R\sigma_{\epsilon f} u$	(70)	Bandwidth of $\dot{\phi}$, $\dot{\theta}$ is $a = 0.1$ rad/s; $\alpha = 2a/\omega_s = 1.34$	796*
σ_x^T—Total rms position error, at 1 h					2210

[a] Performance values for a modern dry tuned rotor gyroscope.
[b] $\dot{\psi}_d$ in AZG is assumed to degrade to ~0.1 deg/h as a result of increased gyro torquer activity.

$$\Delta x = R\epsilon_i (1 - \cos\zeta) \tag{77}$$

I. Vibro-Pendulous Effect

The relatively narrow bandwidth of 5 Hz of the closed-loop system may cause a bias of about 100 μg if it is exposed to a persisting 1 g, 100-Hz vibration inclined at 45 deg to the vertical.

J. Summary of Error Analysis

A numerical error evaluation based on the foregoing error propagation models and on typical data of a DTR gyro are summarized in Table 1. Only the most significant error components marked by * are shown in Fig. 6 as a function of time up to 2 h. They are considered as statistically independent. The total rms position error denoted by σ_x^T is also presented in Fig. 6, showing that at 1 h, the positional error is 2200 m, or 1.2 n.mi. The inclusion of a constant 100-μg bias due to the vibropendulous effect would cause an error of the same form, as shown by curve 12 in Fig. 6, and would increase σ_x^T by approximately 10%. Other assumptions for ϵ_i and alternative models for temperature variation exhibit a similar trend for σ_x^T and only a minor change in it at 1 h. The results are shown in Figs. 7 and 8.

VII. Conclusions

It has been shown that, within the limitations assumed for acceleration and attitude variations, an inertial navigation system can be mechanized with a pendulous structure which dispenses with conventional accelerometers, thus achieving significant savings in components and system complexity. The primary contributors to the positional error up to 1 h are drift of the levelling gyro due to temperature variations, gyrocompassing error, and azimuth gyro drift. The estimated error budget shows that positional accuracy is in the order of 1-2 n.mi. Though apparently not dominant, the effects of dimensional stability with temperature variations and gimbal torquer nonlinearities should be observed in possible future experimental work.

Acknowledgments

This research was carried out under a National Research Council Associateship at NASA-Ames Research Center.

References

[1] Garg, S.C., Morrow, L.D., and Mamen, R., "Strapdown Navigation Technology: A Literature Survey," *Journal of Guidance and Control,* Vol. 1, May-June 1978, pp. 161-172.

[2] Peterson, R., "Advantages of Gimballed Inertial Navigation Systems," *NAECON Proceedings,* 1976, pp. 508-513.

[3] Farrell, J.L., *Integrated Aircraft Navigation,* Academic Press, New York, 1976, pp. 104-105.

[4] Bryson, A.E., "Kalman Filter Divergence and Aircraft Motion Estimators," *Journal of Guidance and Control,* Vol. 1, Jan.-Feb. 1978, pp. 71-79.

[5] Monaco, S.R., and Audly, D.R., "Schuler Tuned Vertical Indicating System," *Journal of Guidance and Control,* Vol. 1, Nov.-Dec. 1978, pp. 413-419.

[6] Hector, F., "The Ramp Inertial Navigation System," *Philips Technical Review,* Vol. 29, Nos. 3-4, 1968, pp. 69-85.

[7] Astrom, K.J., and Hector, N.F., "Vertical Indication with a Physical Pendulum Based on Electromechanical Synthesis of a High Moment of Inertia," Division of Applied Hydromechanics, Royal Institute of Technology, Stockholm, Sweden, Rept. No. 59082-TTN Group, Aug. 1959.

[8] Koenke, E.J., "Analysis and Evaluation of a Novel Inertial Navigation System," NASA TN D-5456, Nov. 1969.

[9] Craig, R.J.G., "Theory of Operation of an Elastically Supported Tuned Gyroscope," *IEEE Transactions on Aerospace and Electronic Systems,* Vol. AES-8, No. 3, May 1972, pp. 280-288.

[10] Ronald, N.A. and Maunder, L., *Gyrodynamics and Its Engineering Applications,* Academic Press, New York, 1961, Chap. 12.

[11] Kayton, M. and Fried, W.R., *Avionics Navigation Systems,* Wiley, New York, 1969, Chap. 7, p. 323.

[12] Heffley, R.K., "A Study of Key Features of Random Atmospheric Disturbance Models for the Approach Flight Phase," *Proceedings of the AIAA Atmospheric Flight Mechanics Conference,* Aug. 1977, pp. 219-228.

[13] Melsa, J.L. and Sage, A.P., *An Introduction to Probability on Stochastic Processes,* Prentice Hall, New York, 1973, Chap. 5.

[14] Gelb, A. and Vander Velde, W.E., *Multi-Input Describing Functions and Nonlinear Systems Design,"* McGraw-Hill, New York, 1968.